Acidified seawater impacts sea urchin larvae pH regulatory systems relevant for calcification

Meike Stumpp[a,b,c,1], Marian Y. Hu[a,b,c,1], Frank Melzner[b], Magdalena A. Gutowska[a,b], Narimane Dorey[c], Nina Himmerkus[a], Wiebke C. Holtmann[a], Sam T. Dupont[c], Michael C. Thorndyke[c], and Markus Bleich[a,2]

[a]Institute of Physiology, Christian Albrechts University Kiel, 24098 Kiel, Germany; [b]Helmholtz Centre for Ocean Research Kiel (GEOMAR), 24105 Kiel, Germany; and [c]Department of Biological and Environmental Sciences, The Sven Lovén Centre for Marine Science, University of Gothenburg, Kristineberg, 45178 Fiskebäckskil, Sweden

Edited by George N. Somero, Stanford University, Pacific Grove, CA, and approved September 19, 2012 (received for review June 22, 2012)

Calcifying echinoid larvae respond to changes in seawater carbonate chemistry with reduced growth and developmental delay. To date, no information exists on how ocean acidification acts on pH homeostasis in echinoderm larvae. Understanding acid–base regulatory capacities is important because intracellular formation and maintenance of the calcium carbonate skeleton is dependent on pH homeostasis. Using H^+-selective microelectrodes and the pH-sensitive fluorescent dye BCECF, we conducted in vivo measurements of extracellular and intracellular pH (pH_e and pH_i) in echinoderm larvae. We exposed pluteus larvae to a range of seawater CO_2 conditions and demonstrated that the extracellular compartment surrounding the calcifying primary mesenchyme cells (PMCs) conforms to the surrounding seawater with respect to pH during exposure to elevated seawater *p*CO_2. Using FITC dextran conjugates, we demonstrate that sea urchin larvae have a leaky integument. PMCs and spicules are therefore directly exposed to strong changes in pH_e whenever seawater pH changes. However, measurements of pH_i demonstrated that PMCs are able to fully compensate an induced intracellular acidosis. This was highly dependent on Na^+ and HCO_3^-, suggesting a bicarbonate buffer mechanism involving secondary active Na^+-dependent membrane transport proteins. We suggest that, under ocean acidification, maintained pH_i enables calcification to proceed despite decreased pH_e. However, this probably causes enhanced costs. Increased costs for calcification or cellular homeostasis can be one of the main factors leading to modifications in energy partitioning, which then impacts growth and, ultimately, results in increased mortality of echinoid larvae during the pelagic life stage.

pH microelectrode | *Strongylocentrotus droebachiensis* | acid–base regulation | Na^+-HCO_3^- transport | epithelial transport

Sea urchin larvae have been shown to react with particular sensitivity to CO_2-induced reductions in seawater pH (1–4). When larvae are chronically exposed to elevated seawater *p*CO_2 of >0.1 kPa, e.g., as is predicted to occur during the next century in response to anthropogenic CO_2 emissions or through upwelling of low-pH deep water, this sensitivity is reflected in reduced growth and developmental rates (5, 6). Echinoderm larvae are considered to be especially vulnerable to seawater pH reduction and to the associated changes in calcium carbonate saturation state of seawater (Ω_{Cal}) because their internal skeleton is composed of high magnesium calcite, a highly soluble form of $CaCO_3$ (7, 8). However, long-term reductions in growth and development might just as well be evoked by other physiological mechanisms that are also sensitive to hypercapnia and the related acid–base disturbances. Recent studies conducted on several marine taxa including mollusks (9) and echinoderms (10) demonstrated increased metabolic rates in response to elevated seawater *p*CO_2. It was concluded that reductions in somatic growth and rate of development were caused by a shift of energy partitioning toward vital functions such as cellular acid–base homeostasis (9, 10). For example, sea urchin larvae exposed to acidified seawater (0.35 kPa CO_2, pH 7.25) maintained a fully calcified larval phenotype, albeit at a reduced rate of body growth (4). This indicates that biomineralization mechanisms remain functional despite CO_2-induced changes in the seawater carbonate system.

The calcification process in sea urchin larvae has been well investigated (e.g., refs. 7, 11–14). Primary mesenchyme cells (PMCs), located within the extracellular matrix of the primary body cavity, form a syncytium around the growing spicules of the pluteus larvae. This syncytial sheath covers the entire surface of the spicules and communicates with the extracellular environment of the primary body cavity (8, 15). The high magnesium calcitic spicules are formed through the production of a transient amorphous calcium carbonate (ACC) phase within vesicles in PMCs. ACC is subsequently released into the spicular cavity (7, 8, 12, 16). To fuel the calcification process, bicarbonate (HCO_3^-) is absorbed from the seawater (40%) as well as generated from metabolic CO_2 (60%) (11). On the other hand, Ca^{2+} is exclusively obtained directly from the seawater (13). Although the general principle of calcification is well understood, mechanistic information concerning the nature of the transporters that facilitate Ca^{2+} or HCO_3^- uptake in PMCs is limited. Several pharmacological studies suggested that Ca^{2+} channels and transporters are key players in the provision of Ca^{2+} for spicule formation (17, 18). To remove protons generated during $CaCO_3$ precipitation, PMCs must possess efficient acid–base regulatory properties (19, 20). However, the mechanistic basis of acid–base regulation in PMCs has not been explored so far. Typically, a cell is required to secrete acid equivalents (e.g., H^+) or to increase intracellular buffering capacity via the import of buffers (e.g., HCO_3^-) to compensate for an intracellular acidosis. Acid–base equivalent transport is facilitated through ion transporters such as Na^+/H^+ exchangers (NHEs), Na^+-dependent HCO_3^- transporters of the SLC4 transporter family, or primary active transporters (e.g., V-type H^+-ATPases) (21, 22).

Here, we investigate how changes in seawater *p*CO_2 affect the direct environment of the calcifying PMCs and whether sea urchin larvae are able to regulate extracellular pH in response to both acute and chronic seawater acidification. Furthermore, we study acid–base regulatory features of the PMCs to provide information on the extent and mechanisms of intracellular pH regulatory abilities. This knowledge is crucial to understand the mechanisms underlying the control of pH homeostasis in PMCs and, thus, calcification during environmental hypercapnia. We hypothesize that a higher fraction of energy spent on acid–base compensatory processes of PMCs in response to CO_2-induced

Author contributions: M.S., M.Y.H., F.M., M.A.G., N.H., and M.B. designed research; M.S., M.Y.H., F.M., M.A.G., N.D., N.H., W.C.H., and M.B. performed research; F.M., M.A.G., W.C.H., S.T.D., M.C.T., and M.B. contributed new reagents/analytic tools; M.S., M.Y.H., F.M., M.A.G., N.D., N.H., and M.B. analyzed data; and M.S., M.Y.H., F.M., M.A.G., N.H., S.T.D., M.C.T., and M.B. wrote the paper.

The authors declare no conflict of interest.

This article is a PNAS Direct Submission.

[1]M.S. and M.Y.H. contributed equally to this work.

[2]To whom correspondence should be addressed. E-mail: m.bleich@physiologie.uni-kiel.de.

This article contains supporting information online at www.pnas.org/lookup/suppl/doi:10.1073/pnas.1209174109/-/DCSupplemental.

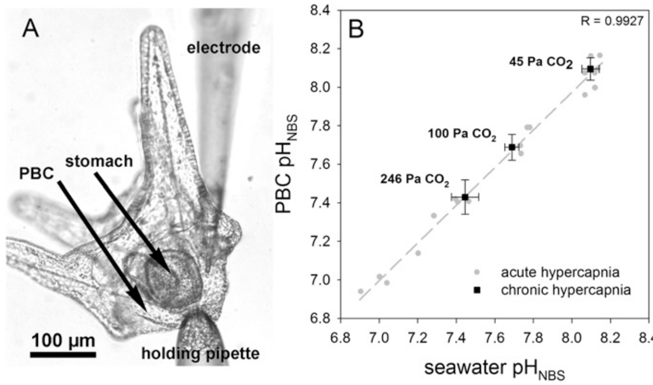

Fig. 1. (*A*) *S. droebachiensis* pluteus larvae attached to the holding pipette and the tip of the measuring electrode inside the primary body cavity (PBC). (*B*) Relationship between seawater and the PBC pH (NBS scale) during acute and chronic environmental hypercapnia. Bars represent ±SD; n = 4–5.

seawater acidification may be a critical reason for the reported reductions in growth and development of echinoid larvae.

Results and Discussion

Lack of pH Regulation Within the Primary Body Cavity. H^+-selective microelectrodes were adapted for extracellular pH (pH_e) measurements in marine invertebrate larvae. Surprisingly, pH_e in the body cavity followed seawater pH (pH_{sw}) without any measurable signs of active pH_e compensation. This observation was independent of acute or chronic exposure to elevated seawater pCO$_2$ (Fig. 1). Additionally, pH_e was also monitored noninvasively in larvae loaded with the pH-sensitive dye 2′,7′-bis-(carboxyethyl)-5(6)-carboxyfluorescein (BCECF) in an experiment to validate our electrode measurements. These measurements confirmed the lack of significant pH_e regulatory ability (Fig. S1). A bias on pH electrode measurements was excluded by performing nonselective voltage electrode measurements. No transepithelial potential difference was recorded between the bath solution and extracellular matrix (Fig. S2). The lack of any difference in pH_{sw} vs. pH_e is surprising because it would indicate very shallow pCO$_2$ diffusion gradients from the extracellular compartment to the seawater. Typically, pCO$_2$ values in extracellular fluids of heterotrophic marine metazoans are at least 0.1 kPa higher than those of the surrounding seawater, thereby enabling diffusive CO_2 excretion across a delimitating barrier, thus rendering pH_e more acidic than seawater (23). The pluteus ectoderm is very thin (~1–2 µm) (Fig. 2*E*), comparable in thickness to respiratory epithelia of, e.g., teleost fish (23), thus enabling shallow diffusion gradients for pCO$_2$. However, the relatively high pH_e within the body cavity in our measurements could also be related to an ectoderm that is leaky for ions and small molecules. Using fluorescein-5-isothiocyanate (FITC) dextran conjugates of different molecular weights, we studied the permeability of the larval ectoderm. We exposed four-armed pluteus larvae to FITC dextran-containing seawater (Fig. 2) and found that free FITC (M_r = 0.4 kDa) equilibrated within 15 min with the extracellular matrix (ECM). Significant entry of FITC dextran conjugates of 4 kDa (15-, 60-min incubation) and 10 kDa (60-min incubation) and the absence of entry of 40-kDa particles within the 60-min incubation period (Fig. 2 *A* and *B*) indicated a comparatively high permeability of the pluteus ectoderm. Because no significant increases in FITC-derived fluorescence were measured in the cytosol of ectodermal or PMC cells (Fig. 2*B*), it appears that equilibration between ECM and seawater is mediated through paracellular pathways. It is likely that the pluteus ectoderm is characterized by a high permeability for ions as well. This assumption is supported by the rapid equilibration of pH_e with pH_{sw} in our experiments: a change in 0.3 pH units in the seawater medium typically resulted in stable pH_e within ~20 s (Figs. S2 and S3).

Sea urchin larvae potentially sacrifice a certain degree of control over the abiotic conditions in the extracellular space to create favorable conditions for calcification (see discussion below). Vital stains using the dye FM1-43 indicate that the mesenchymal cells (PMCs, secondary mesenchyme cells) that populate the ECM are connected via a multitude of filopodia to each other and to cells of the ectoderm and the digestive tract (Fig. 3 and Fig. S4) (24, 25). These filopodial connections, which have been suggested to primarily aid in cell–cell signaling (e.g., refs. 26, 27), might also fulfill roles related to nutrient distribution that are classically mediated by the extracellular fluid in most adult invertebrates. This suggests that sea urchin larvae shift nutrient distribution to cellular syncytia to use the extracellular space more efficiently for the demands of ionic exchange processes relevant for calcification.

Chronically Elevated Seawater pCO$_2$ Directly Affects the Sites of Calcification. The present work demonstrates that, even under chronically decreased seawater pH, the primary body cavity conforms in pH with the environment. Under control conditions, a comparatively high pH_e (>8.1) in comparison with other marine invertebrates (28) might be beneficial for maintenance of the endoskeleton. Because the larval spicules are surrounded by sheaths of the PMC syncytium that do not fully isolate them from the extracellular medium (8, 15), high pH_e will enable a comparatively high $CaCO_3$ saturation state in the direct vicinity of the spicules. On the other hand, uncompensated pH_e during chronic acid challenge might lead to an increased energy demand for the PMCs to prevent dissolution of formed spicules within their sheaths when Ω decreases below 1. For example, Clark et al. (29) observed corrosion of larval spicules in *Evechinus chloroticus* and *Pseudechinus huttoni*

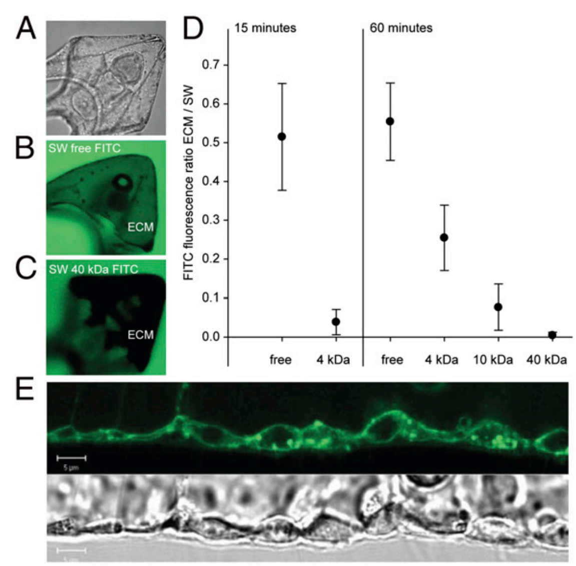

Fig. 2. Determination of epithelial permeability in pluteus larvae in vivo using FITC dextran conjugates of varying molecular weights and confocal microscopy. (*A*) Transmission image of pluteus larva; (*B*) confocal image of larva in a similar position as in *A* exposed to 4-kDa FITC dextran in seawater for 60 min; the green color in the extracellular matrix (ECM) indicates equilibration of FITC dextran between surrounding seawater (SW) and ECM; (*C*) confocal image of larva exposed to 40 kDa for 60 min; the dark color indicates lack of equilibration of FITC dextran between ECM and SW. (*D*) Equilibration of FITC dextrans of varying molecular weights between SW and ECM following 15- and 60-min incubation. Equilibration is represented as the ratio of FITC fluorescence within the ECM and the SW surrounding the larva. Low values indicate a low permeability. (*E*) Corresponding confocal (FM1-43-stained) and transmission images of the pluteus larva outer epithelium. Bars represent ±SD; n = 9.

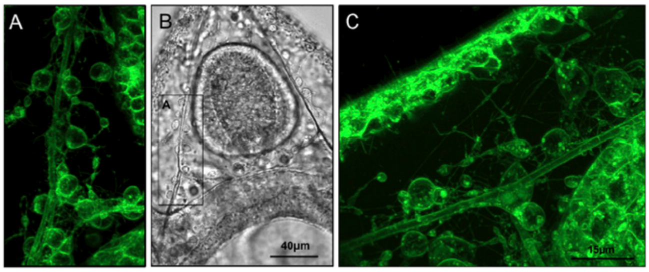

Fig. 3. In vivo confocal images of pluteus larvae using the vital dye FM1-43 that stains membranes. Primary mesenchyme cell (PMC) syncytia and their sheaths, as well as filopodia connecting them with each other and epithelial cells are visible, as are vesicles within cells and filopodial connections. *A* is a close-up confocal image of the region depicted in the *Inset* in the transmission image (*B*). *C* depicts a similar region from a different larva as shown in *A* and *B*, but rotated by 90° clockwise.

pluteus larvae during exposure to pH 7.7 and 7.6, respectively. However, it has been demonstrated that sea urchin larvae are capable of maintaining calcification rates under acidified conditions when calcification rates are normalized to growth rate (4). Thus, pH conformity of the primary body cavity with the surrounding seawater suggests that PMCs themselves must have the ability to control intracellular pH, as well as pH in the microenvironment surrounding the spicules to at least partially protect the spicules from dissolution.

pH_i Regulatory Abilities of PMCs. To test whether PMCs themselves are able to control pH_i—necessarily linked to calcification and skeletogenesis—we measured their pH_i regulatory capacity using the fluorescent pH-sensitive dye BCECF (Fig. 4 and Fig. S5). Using pulses of NH_3/NH_4^+ solution, we demonstrated pH_i regulatory abilities in PMCs (Fig. 4*A*). Under control conditions (pH_{sw} 8.1), PMCs of five larvae were characterized by a control ratio of 1.41 ± 0.06, which corresponds to a pH_i of 6.9 as determined by nigericine calibration (Fig. 4*B*). pH_i values for sea urchin eggs a few minutes to hours postfertilization were reported to range between 6.8 and 7.3 depending on the method and species used (30, 31). The initial alkalization of fertilized sea urchin eggs has been hypothesized to be one of several signals inducing protein synthesis and cell functionality (32, 33). pH_i values for marine invertebrates were reported to range from 6.9 to 7.4 depending on species and methods used (34–38). The 20 mM NH_3/NH_4^+ solution induced an intracellular alkalinization leading to an increase of pH_i by ∼0.2 ratio units corresponding to a ΔpH of 0.7. After washout of the NH_3/NH_4^+ solution, pH_i rapidly dropped by ∼0.7 pH units below the control value, followed by a pH compensation reaction to control levels within 15 min (Fig. 4). Buffering capacity (β) (mmol·L^{-1}·pH $unit^{-1}$, slykes) of PMCs was calculated according to Graber et al. (39) by dividing the amount of acid load by the measured change of pH_i produced by this load. β values obtained for PMCs under control conditions were 20.83 ± 7.78 slykes (n = 9). This buffering capacity is comparable with that of other invertebrates, which were typically reported to be in the range of 16–40 slykes (37, 38, 40–42). Rates of pH_i compensation are about five to seven times slower than recovery times reported for strong ion regulatory cells of rat epithelia [2-3 min in colon or Henle's loop cells (22, 43–45)] but comparable with the recovery rate of crayfish neurons exposed to a similar protocol [∼20 min (46)], indicating a significant acid–base regulatory capacity in echinoid PMCs.

Na^+-Dependent pH_i Regulation in PMC. The pH_i regulatory machinery has been widely characterized for various animal cell types and is essential for the maintenance of enzyme functionality and cellular processes (for a review, see ref. 22). In general, cells maintain pH homeostasis by the import/export of protons and anionic buffers (e.g., HCO_3^-) (47). Our current data clearly indicate that the compensation reaction after NH_3/NH_4^+-induced acidosis in PMCs is highly dependent on Na^+ and HCO_3^- transport (Fig. 5 and Table S1, including baseline pH, pH values after NH_3/NH_4^+ pulse, and recovery rate). Compared with control conditions, the pH_i recovery rate was reduced by 68% in the presence of 5 mM Na^+ and by 74% in a HCO_3^--free solution (Fig. 5 *A* and *C* and Table S1). This suggests the involvement of Na^+-dependent HCO_3^- import mechanisms during pH recovery, which are an indirect sink of ATP. Transporters of the SLC4 family, including Na^+/HCO_3^- cotransporters and Na^+-dependent Cl^-/HCO_3^- exchangers were widely identified as key players in this regulatory process (21, 48–50). The sea urchin PMC transcriptome contains a large number of genes coding for ion transporters including Na^+/K^+-ATPase (NKA), Na^+/HCO_3^- cotransporters (NBC), H^+-ATPases (HA), and NHEs (51). This indicates that PMCs possess the necessary molecular machinery to regulate pH_i by means of proton secretion and HCO_3^- accumulation. However, besides the importance of Na^+-dependent HCO_3^- import in PMCs, the present work also suggests that amiloride-sensitive proton extrusion mechanisms are probably not the major compensation pathway in response to an intracellular acidosis. Although a significant reduction in the extent of recovery in pH_i was observed in the presence of 100 μM amiloride (to 45% of control pH_i/ratio) (Fig. 5*B*), the slope of the recovery reaction was not significantly different from that under control conditions (Fig. 5*C*). Because nonmammalian NHEs were demonstrated to be less sensitive to amiloride, with some NHEs being insensitive up to concentrations of 500 μM (52), this experiment cannot provide definitive answers to the role of NHE proteins in PMC pH regulation. However, because protons are generated during the calcification process within the PMCs (20, 53), the identification and characterization of other acid secretion mechanisms involving transporters such as the

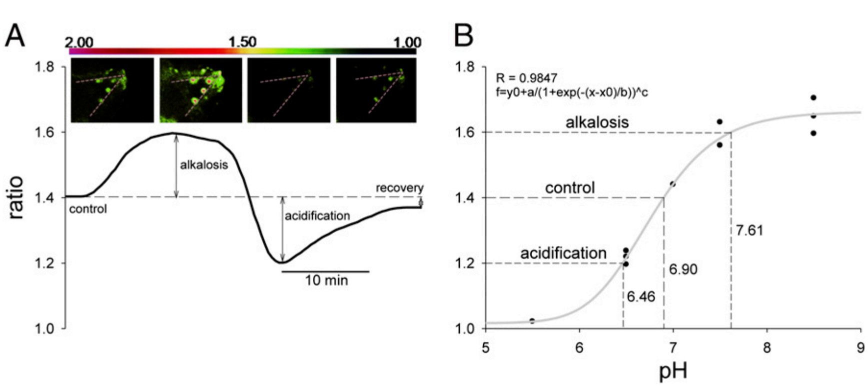

Fig. 4. Ratiometric fluorimetry in PMCs using the pH-sensitive dye BCECF-AM. (*A*) Schematic illustration of a recording trace including ratio images (*Top*: the dashed lines represent the orientation of spicules). Data were obtained from the control period (control), after addition and removal of NH_3/NH_4^+ (alkalosis and acidification; ammonium pulse), and during pH_i recovery. (*B*) Calibration curve of BCECF-AM in PMCs fitted by a function that flattens toward more acidic or alkaline conditions allowing the translation of ratios to pH values.

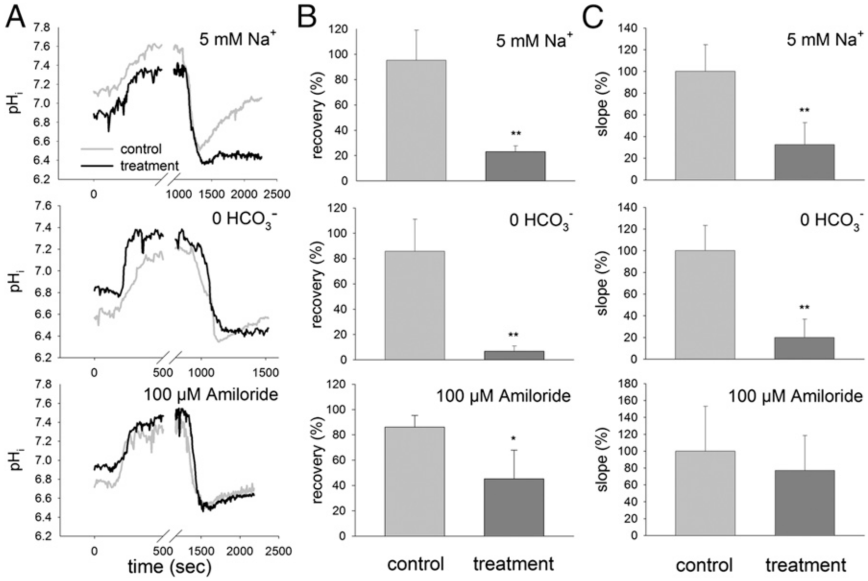

Fig. 5. Acid–base regulatory abilities of PMCs in the presence of low (5 mM) Na^+, without HCO_3^- and with 100 μM amiloride. (*A*) Original recordings of control and treatment traces representing average values of four to five single measurements. Presence of NH_3/NH_4^+-induced alkalosis and the washout-induced acidosis under the three experimental conditions. (*B*) The recovery given in percentage of the initial value, before alkalosis in response to control and treatment conditions. (*C*) Recovery rate represented by the compensatory slope after acidosis given in percentage of the control (100%) value, in response to control and treatment conditions. Bars represent ±SD; *n* = 4–5.

V-type H^+-ATPase or H^+/K^+-ATPase is an important task in further investigations.

Conclusion. Gene expression analysis of sea urchin larvae reared under acidified conditions revealed an increased expression of NKA α-subunit, the key enzyme that provides the electrochemical gradient for most secondary active transport processes (4, 54, 55). This up-regulation of NKA is accompanied by an increase in metabolic rate, indicating a higher energy demand during environmental hypercapnia (10, 54). Because up to 77% of larval metabolism in sea urchin pluteus larvae is required to fuel the energetic demands of NKA under control conditions (56), it is likely that additional acid–base stress will significantly impact the organism's energy budget. We suggest that a higher fraction of energy is spent on PMC acid–base regulation because these have to maintain full cell functionality in a more acidified extracellular medium. Thus, calcification during environmental hypercapnia could impact energy allocation. Because vesicular ACC precipitation occurs intracellularly in PMCs (8), the processes of pH_i regulation and calcification are intrinsically linked: membrane transporters that are involved in ACC precipitation depend on H^+ and HCO_3^- concentrations in the cytosol, which in turn depend on the action of the pH_i regulatory machinery (summarized in Fig. 6). In this way, our data support the concept that maintenance of calcification rates in sea urchin larvae under elevated seawater pCO_2 is primarily an energetic, rather than a physicochemical problem. This helps to explain the observed phenomenon of an altered energy allocation under acidified conditions. Decreases in larval developmental rates and delays in metamorphosis will likely result in a higher mortality during the planktonic life phase (57–59). Furthermore, because the energy reserves required by the juvenile sea urchin to support the first weeks after metamorphosis are accumulated by the larvae (60), energetic compromises faced by larval stages may translate into juvenile fitness problems and thus will define the long-term fate of these keystone species in future marine habitats.

Materials and Methods

Sea Urchin Larvae Culture and CO_2 Perturbation Experiment. All animal experiments were performed according to the German law for animal welfare and were approved by the animal welfare officer of the Christian Albrechts University, Kiel. Adult *Strongylocentrotus droebachiensis* were collected in Winter 2010 and 2011 in the Kattegat (Dröbak, Norway) by divers. Spawning was induced by injection of 2 mL of 0.5 mM KCl into the coelomic cavity. For each experiment, eggs of one to two females were collected in separate 1-L beakers, washed, and fertilized by adding dry sperm (20 μL) of two males. Fertilization was followed by monitoring the fertilization-induced elevation of the oocyte membrane under a stereomicroscope (fertilization rates, >95%). Zygotes were allowed to divide once before they were pooled, concentrated in 25 mL, and split into 2-L (three replicates per pCO_2 treatment, Erlenmeyer flasks) culture vessels, which were preequilibrated at three different pCO_2, control (~0.05 kPa, pH 8.1), intermediate (0.12 kPa, pH 7.7), and high pCO_2 (~0.24 kPa, pH 7.4) by a central automatic gas mixing facility (Linde Gas, HTK Hamburg, Germany). Water pH_{NBS}, salinity, and temperature were monitored daily in the setup during the entire incubation period. Seawater samples (0.5 L) for determination of

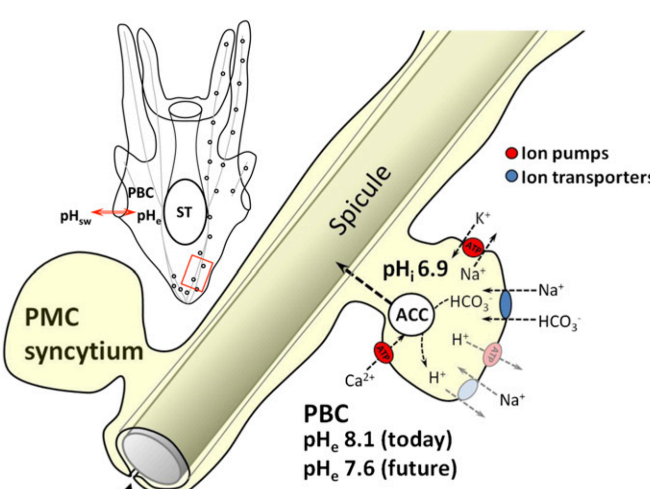

Fig. 6. Schematic model summarizing the interplay of calcification, pH regulation, and energetic costs in sea urchin larvae during environmental acidification. The primary body cavity (PBC) pH conforms to the surrounding seawater pH (pH_{sw}). A decrease in pH_e directly affects the calcifying primary mesenchyme cell (PMC) syncytia challenging the intracellular pH (pH_i) regulatory machinery due to decreased proton gradients. The vesicular precipitation of amorphous calcium carbonate (ACC) within PMCs is intrinsically linked to pH_i regulation. pH homeostasis is maintained by ion transporters, which either directly or indirectly depend on the consumption of energy. Increased energetic costs due to decreased proton gradients lead to a shift in the larvae's energy budget, which decreases scope for growth and may also translate into juvenile impaired fitness. ST, stomach; putative transporters are in gray.

PHYSIOLOGY

total dissolved inorganic carbon, C_T, were collected weekly. C_T was determined using an AIRICA analyzer (Marianda). C_T was corrected using certified reference material provided by Andrew Dickson (Scripps Institution of Oceanography, La Jolla, CA) (61). Seawater carbonate system speciation was calculated from pH_{NBS} and C_T with the open-source program CO2SYS (62) using the dissociation constants by Mehrbach et al. (63) as refitted by Dickson and Millero (64). Water parameters measured during the experimental period are summarized in Table S2.

Larval culturing and monitoring was essentially conducted as described in previous studies (10, 54).

Selective Ion Electrode Technique. Selective ion electrode measurements were essentially performed after Kuehl and Revsbech (65) to measure H^+ concentrations in the extracellular gel matrix (ECM) of sea urchin larvae. Glass capillary tubes (borosilicate; inner diameter, 1.2 mm; outer diameter, 1.5 mm; Hilgenberg) were pulled on a DMZ-Universal puller (Zeitz Instruments) into micropipettes with tip diameters of 2–3 μm. These were then baked at 200 °C for 4 h and vapor-silanized with dimethyl chlorosilane (Sigma-Aldrich) overnight. The micropipettes were front-loaded with a 200-μm column of liquid ion exchanger mixture (H^+ ionophore III; Sigma-Aldrich) diluted in 2-nitrophenyl ether at a concentration of 10.5 $mg \cdot mL^{-1}$. Additionally, micropipettes were again front-loaded with a 100-μm column of the ionophore mixture containing a polyvinylchloride/tetrahydrofuran (330 $mg \cdot mL^{-1}$) solution with a ratio of 1:3 to seal the opening of the electrode tip. The micropipette was backfilled with a 4-cm column of pH electrolyte solution (300 mM KCl, 50 mM $NaPO_4$, pH 7) to create an ion selective microelectrode (probe). To calibrate the ion-selective probe, the Nernstian property of each microelectrode was measured by placing the microelectrode in a series of artificial seawater (ASW) solutions (pH 6, 7, 8, and 9) with reference to an Ag/AgCl electrode. By plotting the voltage output of the probe against log $[H^+]$ values, a linear regression yielded a Nernstian slope of 49.8 ± 2.3 mV (n = 12) for 1 pH unit. With this method, we were able to resolve a minimum difference of 0.1 pH units (corresponding to a change in pCO_2 of ∼0.02–0.04 kPa). Electrode response times in the perfusion solution (0.79 ± 0.21 $s \cdot nM\ [H^+]^{-1}$) and within the primary body cavity (1.75 ± 0.42 $s \cdot nM\ [H^+]^{-1}$) were calculated by the time needed to reach 95–100% of the fully stabilized value after a pH change (usually 0.3 or 0.4 pH units between pH 8.1, 7.7, and 7.4) in the perfusion bath.

Measurement of Extracellular H^+ Concentrations. The electrode measurements were performed at 10 °C on an inverse microscope (Axiovert 135; Zeiss) equipped with a temperature-controlled perfusion system, allowing the quick exchange of different pH solutions inside the perfusion chamber. The pH of the bath solutions was adjusted by equilibrating ASW with pure CO_2 to the desired pH. The larva was placed inside the perfusion bath and kept in position via a holding pipette (30- to 40-μm tip diameter) to which a slight vacuum was applied. The ion-selective probe was mounted on a remote-controlled micromanipulator (Phytron) and was introduced into the ECM from the base of the arms at the oral side of the larvae (10–20 μm inside the ECM) to record the ionic activities (Fig. 1*A*). The epidermis and basal lamina formed a seal around the entrance point of the electrode, preventing fluid exchange between seawater and the primary body cavity. pH recordings were performed on pluteus larvae [8–10 d postfertilization (dpf)] reared under control conditions, which were exposed to acute changes in seawater pH ranging from 6.9 to 8.2. Furthermore, the same measurements were also performed on pluteus larvae (8–10 dpf) from the CO_2 perturbation experiment to address the effects of chronically elevated seawater pCO_2 on extracellular pH homeostasis.

Visualization of Mesenchyme Cell Filopodial Network. Four-armed pluteus larvae (96 h) were incubated for 15 min in control (pH 8.1) seawater with 20 μM FM1-43 at 10 °C. Following incubation, larvae were placed on microscopy slides suspended in the incubation solution and covered with glass coverslips supported by ∼100-μm-thick fibers as spacers. Larvae were then imaged with a Zeiss LSM510 using a Plan Neofluar 40×/1.3 objective and a 505-nm long-pass filter at an excitation wavelength of 488 nm. Images were collected within 20 min (n = 20) at room temperature (20 °C).

Epithelial Permeability Measurements with FITC Dextran. To measure epithelial permeability, four-armed pluteus larvae (96 h) were incubated for 15 and 60 min in control (pH 8.1) seawater with 0.4 mM FITC dextran (free FITC, 0.4, 4, 10, 40 kDa; Sigma-Aldrich) at 10 °C. FITC dextran solutions were dialyzed overnight in ASW in MWCO-dialysis tubing (Roth) before experiments. Following incubation, larvae were imaged on a Zeiss LSM510 as described above. Images were collected within 10 min (n = 9 larvae per treatment) at room temperature (20 °C).

Bag Isolation Procedure and Dye (BCECF-Acetoxymethylester) Loading. To measure PMC intracellular pH (pH_i), epidermal cells of 8–10 dpf larvae were removed according to Harkey and Whiteley (66). Using this protocol, both epithelial as well as PMCs can be maintained viable for hours (66). Larvae were incubated at 10 °C with a final concentration of 50 $\mu mol\ L^{-1}$ BCECF-acetoxymethylester (BCECF-AM) for 30 min to allow sufficient uptake and cleavage of the esterified dye by intracellular esterases. Thereafter, only larvae, which were firmly attached to the perfusion bath bottom, were used for measurement. The flow rate of the perfusion solutions was 2–3 $mL \cdot min^{-1}$. With this dye-loading procedure, we achieved a signal-to-noise ratio for the emission signal of >10 throughout an experimental period of >2 h without appreciable loss of signal intensity.

Solutions. ASW solutions were mixed according to Zeebe and Wolf-Gladrow (67). Osmolality (980 ± 10 $mosm \cdot kg^{-1}$) and salinity (31 ± 1) were chosen to match the natural seawater used in the larval cultures. All ingredients of the experimental solutions are given in Table S3. Amiloride was added at a final concentration of 100 μM to the ASW. DMSO did not exceed a concentration of 0.1%.

Microfluorimetry. Fluorescence was monitored with an imaging system (Visitron). The dye was alternatively excited at a rate of 0.2 Hz at 486 and 440 nm (±10-nm bandwidth) for 24 and 60 ms, respectively. Emission was recorded at 525 nm (±13-nm bandwidth), and the integrated ratio of the emission intensities at the two excitation wavelengths over the whole cell was calculated after subtraction of system immanent camera offset and background signal (MetaFluor Software 7.6.1; Molecular Devices). From each larva, the recordings of four to five PMCs were averaged and treated as one replicate (n = 1). Four to five control and treatment larvae were measured in an alternate mode and used for further analysis. Nigericin was used to calibrate pH_i of living cells as previously described by Suffrian et al. (68). PMCs of pluteus larvae were exposed to 10 $\mu mol \cdot L^{-1}$ nigericin in the presence of 150 $mmol \cdot L^{-1}$ K^+ at pH 5.5, 6.5, 7, 7.5, and 8.5. This $[K^+]_i$ is in the same range reported for fertilized and unfertilized sea urchin eggs (69) and intestinal tissues of the sea urchin *S. droebachiensis* (70). The calibration curve (Fig. 4) allowed estimation of the relationship between detected emission ratio of BCECF and the respective pH_i. A change of 0.1 ratio units corresponded to a change of 0.35 pH units.

For all experiments, the bath was exchanged at a rate of 2–3 $mL \cdot min^{-1}$ at 10 °C, and pH_i was continuously monitored. All larvae were exposed to ASW followed by the 20 mM NH_3/NH_4^+ prepulse. Acidosis was induced by NH_3/NH_4^+ washout using the respective solutions, 5 mM Na^+,HCO_3^--free solutions and ASW plus 100 μM amiloride or control solutions (e.g., ASW or ASW plus DMSO), which were directly applied to the larvae via the perfusion system.

Traces of intracellular pH measurements were analyzed according to the parameters depicted in Fig. 3*A*. To determine the ability of PMCs to recover from an NH_3/NH_4^+-induced acidosis, we calculated the ratio of the recovery value (in the stationary phase of the recovery phase) and the initial control value. Additionally, the slope of the compensation reaction was used to characterize the rate of recovery after an induced acidosis by determining the change in the ratio as a function of time.

Statistical Analysis. Statistical differences between response times of ion-selective electrode measurements and pH regulatory abilities of PMCs were analyzed with Student t test with significance levels of $P < 0.05$ (*) and $P < 0.01$ (**).

ACKNOWLEDGMENTS. We thank U. Panknin, S. Syré, and A. Cipriano for valuable laboratory help and D. de Beer for advice on pH microsensor techniques. This work was funded by Bundesministerium für Bildung und Forschung Grant 03F0608M [Biological Impacts of Ocean ACIDification (BIOACID) 3.1.4] (to F.M and M.B.); by the Linnaeus Centre for Marine Evolutionary Biology, University of Gothenburg (S.T.D.); by a Linnaeus grant from the Swedish Research Councils Vetenskapsrådet and Formas (to M.C.T.); and by Knut and Alice Wallenberg's minnen and the Royal Swedish Academy of Sciences (M.S. and M.C.T.).

1. Dupont S, Ortega-Martínez O, Thorndyke MC (2010) Impact of near-future ocean acidification on echinoderms. *Ecotoxicology* 19(3):449–462.
2. Kurihara H, Shirayama Y (2004) Effects of increased atmospheric CO_2 on sea urchin early development. *Mar Ecol Prog Ser* 274:161–169.

3. O'Donnell MJ, Hammond LM, Hofmann GE (2009) Predicted impact of ocean acidification on a marine invertebrate: Elevated CO_2 alters response to thermal stress in sea urchin larvae. *Mar Biol* 156(3):439–446.
4. Martin S, et al. (2011) Early development and molecular plasticity in the Mediterranean sea urchin *Paracentrotus livid*us exposed to CO_2-driven acidification. *J Exp Biol* 214(Pt 8):1357–1368.
5. Cao L, Caldeira K (2008) Atmospheric CO_2 stabilization and ocean acidification. *Geophys Res Lett* 35:1–5.
6. Caldeira K, Wickett ME (2005) Ocean model predictions of chemistry changes from carbon dioxide emissions to the atmosphere and ocean. *J Geophys Res* 110:1–12.
7. Raz S, Hamilton PC, Wilt FH, Weiner S, Addadi L (2003) The transient phase of amorphous calcium carbonate in sea urchin larval spicules: The involvement of proteins and magnesium ions in its formation and stabilization. *Adv Funct Mater* 13(6): 480–486.
8. Beniash E, Aizenberg J, Addadi L, Weiner S (1997) Amorphous calcium carbonate transforms into calcite during sea urchin larval spicule growth. *Proc Biol Sci* 264: 461–465.
9. Thomsen J, Melzner F (2010) Moderate seawater acidification does not elicit long-term metabolic depression in the blue mussel *Mytilus edulis. Mar Biol* 157(12): 2667–2676.
10. Stumpp M, Wren J, Melzner F, Thorndyke MC, Dupont ST (2011) CO_2 induced seawater acidification impacts sea urchin larval development I: Elevated metabolic rates decrease scope for growth and induce developmental delay. *Comp Biochem Physiol A Mol Integr Physiol* 160(3):331–340.
11. Sikes CS, Okazaki K, Fink RD (1981) Respiratory CO_2 and the supply of inorganic carbon for calcification of sea urchin embryos. *Comp Biochem Physiol A* 70(3): 285–291.
12. Politi Y, et al. (2008) Transformation mechanism of amorphous calcium carbonate into calcite in the sea urchin larval spicule. *Proc Natl Acad Sci USA* 105(45): 17362–17366.
13. Nakano E, Okazaki K, Iwamatsu T (1963) Accumulation of radioactive calcium in the larvae of the sea urchin *Pseudecentrotus depressus*. *Biol Bull* 125(1):125–136.
14. Wilt FH (2002) Biomineralization of the spicules of sea urchin embryos. *Zoolog Sci* 19 (3):253–261.
15. Decker GL, Morrill JB, Lennarz WJ (1987) Characterization of sea urchin primary mesenchyme cells and spicules during biomineralization in vitro. *Development* 101(2): 297–312.
16. Politi Y, Arad T, Klein E, Weiner S, Addadi L (2004) Sea urchin spine calcite forms via a transient amorphous calcium carbonate phase. *Science* 306(5699):1161–1164.
17. Hwang SP, Lennarz WJ (1993) Studies on the cellular pathway involved in assembly of the embryonic sea urchin spicule. *Exp Cell Res* 205(2):383–387.
18. Jayantha Gunaratne H, Vacquier VD (2007) Sequence, annotation and developmental expression of the sea urchin Ca^{2+}-ATPase family. *Gene* 397(1-2):67–75.
19. McConnaughey TA, Whelan JF (1996) Calcification generates protons for nutrient and bicarbonate uptake. *Earth Sci Rev* 41(1–2):95–117.
20. Buitenhuis ET, de Baar HJW, Veldhuis MJW (1999) Photosynthesis and calcification by *Emiliania huxleyi* (Prymnesiophyceae) as a function of inorganic carbon species. *J Phycol* 35(5):949–959.
21. Romero MF, Fulton CM, Boron WF (2004) The SLC4 family of HCO_3^- transporters. *Pflugers Arch* 447(5):495–509.
22. Boron WF (2004) Regulation of intracellular pH. *Adv Physiol Educ* 28(1-4):160–179.
23. Evans DH, Piermarini PM, Choe KP (2005) The multifunctional fish gill: Dominant site of gas exchange, osmoregulation, acid-base regulation, and excretion of nitrogenous waste. *Physiol Rev* 85(1):97–177.
24. Malinda KM, Fisher GW, Ettensohn CA (1995) Four-dimensional microscopic analysis of the filopodial behavior of primary mesenchyme cells during gastrulation in the sea urchin embryo. *Dev Biol* 172(2):552–566.
25. Miller J, Fraser SE, McClay D (1995) Dynamics of thin filopodia during sea urchin gastrulation. *Development* 121(8):2501–2511.
26. Röttinger E, et al. (2008) FGF signals guide migration of mesenchymal cells, control skeletal morphogenesis [corrected] and regulate gastrulation during sea urchin development. *Development* 135(2):353–365.
27. Ettensohn CA (1990) Cell interactions in the sea urchin embryo studied by fluorescence photoablation. *Science* 248(4959):1115–1118.
28. Melzner F, et al. (2009) Physiological basis for high CO_2 tolerance in marine ectothermic animals: Pre-adaptation through lifestyle and ontogeny. *Biogeoscience* 6(10): 2313–2331.
29. Clark D, Lamare M, Barker M (2009) Response of sea urchin pluteus larvae (Echinodermata: Echinoidea) to reduced seawater pH: A comparison among tropical, temperate and polar species. *Mar Biol* 156(6):1125–1137.
30. Johnson CH, Epel D (1981) Intracellular pH of sea urchin eggs measured by the dimethyloxazolidinedione (DMO) method. *J Cell Biol* 89(2):284–291.
31. Johnson JD, Epel D (1976) Intracellular pH and activation of sea urchin eggs after fertilisation. *Nature* 262(5570):661–664.
32. Rees BB, Patton C, Grainger JL, Epel D (1995) Protein synthesis increases after fertilization of sea urchin eggs in the absence of an increase in intracellular pH. *Dev Biol* 169(2):683–698.
33. Grainger JL, Winkler MM, Shen SS, Steinhardt RA (1979) Intracellular pH controls protein synthesis rate in the sea urchine egg and early embryo. *Dev Biol* 68(2): 396–406.
34. Aickin CC, Thomas RC (1975) Micro-electrode measurement of the internal pH of crab muscle fibres. *J Physiol* 252(3):803–815.
35. Venn AA, et al. (2009) Imaging intracellular pH in a reef coral and symbiotic anemone. *Proc Natl Acad Sci USA* 106(39):16574–16579.
36. Wheatly MG, Henry RP (1992) Extracellular and intracellular acid-base regulation in crustaceans. *J Exp Zool* 263(2):127–142.
37. Wisemann RW, Ellington WR (1989) Intracellular buffering capacity in molluscan muscle: Superfused muscle versus homogenates. *Physiol Zool* 62(2):541–558.
38. Pörtner H-O (1990) Determination of intracellular buffer values after metabolic inhibition by fluoride and nitrilotriacetic acid. *Respir Physiol* 81(2):275–288.
39. Graber M, DiPaola J, Hsiang FL, Barry C, Pastoriza E (1991) Intracellular pH in the OK cell. I. Identification of H^+ conductance and observations on buffering capacity. *Am J Physiol* 261(6 Pt 1):C1143–C1153.
40. Zange J, Grieshaber MK, Jans AWH (1990) The regulation of intracellular pH estimated by ^{31}P-NMR spectroscopy in the anterior byssus retractor muscle of *Mytilus edulis* L. *J Exp Biol* 150:95–109.
41. Thomas RC (1976) The effect of carbon dioxide on the intracellular pH and buffering power of snail neurones. *J Physiol* 255(3):715–735.
42. Burton RF (1978) Intracellular buffering. *Respir Physiol* 33(1):51–58.
43. Bleich M, Köttgen M, Schlatter E, Greger R (1995) Effect of NH_4^+/NH_3 on cytosolic pH and the K^+ channels of freshly isolated cells from the thick ascending limb of Henle's loop. *Pflugers Arch* 429(3):345–354.
44. Boron WF, De Weer P (1976) Intracellular pH transients in squid giant axons caused by CO_2, NH_3, and metabolic inhibitors. *J Gen Physiol* 67(1):91–112.
45. Hasselblatt P, Warth R, Schulz-Baldes A, Greger R, Bleich M (2000) pH regulation in isolated in vitro perfused rat colonic crypts. *Pflugers Arch* 441(1):118–124.
46. Moody WJ, Jr. (1981) The ionic mechanism of intracellular pH regulation in crayfish neurones. *J Physiol* 316:293–308.
47. Boron WF (1983) Transport of H^+ and of ionic weak acids and bases. *J Membr Biol* 72 (1-2):1–16.
48. Virkki LV, Choi I, Davis BA, Boron WF (2003) Cloning of a Na^+-driven Cl/HCO_3 exchanger from squid giant fiber lobe. *Am J Physiol Cell Physiol* 285(4):C771–C780.
49. Piermarini PM, Choi I, Boron WF (2007) Cloning and characterization of an electrogenic Na/HCO_3^- cotransporter from the squid giant fiber lobe. *Am J Physiol Cell Physiol* 292(6):C2032–C2045.
50. Henriksen K, Bollerslev J, Everts V, Karsdal MA (2011) Osteoclast activity and subtypes as a function of physiology and pathology—implications for future treatments of osteoporosis. *Endocr Rev* 32(1):31–63.
51. Zhu X, et al. (2001) A large-scale analysis of mRNAs expressed by primary mesenchyme cells of the sea urchin embryo. *Development* 128(13):2615–2627.
52. Harada K, Fukuda E, Hirohashi N, Chiba K (2010) Regulation of intracellular pH by p90Rsk-dependent activation of an Na^+/H^+ exchanger in starfish oocytes. *J Biol Chem* 285(31):24044–24054.
53. Fujino Y, Mitsunaga K, Yasumasu I (1987) Inhibitory effects of omeprazole, a specific inhibitor of H^+, K^+-ATPase, on spicule formation in sea urchin embryos and in cultured micromere-derived cells. *Dev Growth Differ* 29(6):591–597.
54. Stumpp M, Dupont S, Thorndyke MC, Melzner F (2011) CO_2 induced acidification impacts sea urchin larval development II: Gene expression patterns in pluteus larvae. *Comp Biochem Physiol A Mol Integr Physiol* 160(3):320–330.
55. Hu MY, et al. (2011) Elevated seawater PCO_2 differentially affects branchial acid-base transporters over the course of development in the cephalopod *Sepia officinalis*. *Am J Physiol Regul Integr Comp Physiol* 300(5):R1100–R1114.
56. Leong PKK, Manahan D (1997) Metabolic importance of Na^+/K^+-ATPase activity during sea urchin development. *J Exp Biol* 200(Pt 22):2881–2892.
57. Allen JD (2008) Size-specific predation on marine invertebrate larvae. *Biol Bull* 214(1): 42–49.
58. Dupont S, Dorey N, Thorndyke M (2010) What meta-analysis can tell us about vulnerability of marine biodiversity to ocean acidification? *Estuar Coast Shelf Sci* 89(2): 182–185.
59. Hare JA, Cowen RK (1997) Size, growth, development, and survival of the planktonic larvae of *Pomatomus saltatrix* (Pisces: Pomatomidae). *Ecology* 78(8):2415–2431.
60. Byrne M, et al. (2008) Maternal provisioning for larvae and larval provisioning for juveniles in the toxopneustid sea urchin *Tripneustes gratilla*. *Mar Biol* 155(5):473–482.
61. Dickson AG, Afghan JD, Anderson GC (2003) Reference materials for oceanic CO_2 analysis: A method for the certification of total alkalinity. *Mar Chem* 80(2–3):185–197.
62. Lewis E, Wallace D (1998) *Program Developed for CO_2 System Calculations* (Oak Ridge National Laboratory, Oak Ridge, TN).
63. Mehrbach C, Culberson CH, Hawlwy JE, Pytkowicz RM (1973) Measurement of the apparent dissociation constants of carbonic acid in seawater at atmospheric pressure. *Limnol Oceanogr* 18(6):897–907.
64. Dickson AG, Millero FJ (1987) A comparison of the equilibrium-constants for the dissociation of carbonic-acid in seawater media. *Deep-Sea Res* 34(10):1733–1743.
65. Kuehl M, Revsbech NP (2001) *Microsensors for the Study of Interfacial Biogeochemical Processes* (Oxford Univ Press, Oxford).
66. Harkey MA, Whiteley AH (1980) Isolation, culture, and differentiation of echinoid primary mesenchyme cells. *Wilhelm Raux's Arch* 189(2):111–122.
67. Zeebe RE, Wolf-Gladrow DA (2001) *CO_2 in Seawater: Equilibrium, Kinetics, Isotopes* (Elsevier, Amsterdam), p 346.
68. Suffrian K, Schulz KG, Gutowska MA, Riebesell U, Bleich M (2011) Cellular pH measurements in *Emiliania huxleyi* reveal pronounced membrane proton permeability. *New Phytol* 190(3):595–608.
69. Shen SS, Sui A-L (1989) K^+ activity and regulation of intracellular pH in the sea urchin egg during fertilization. *Exp Cell Res* 183(2):343–352.
70. Lange R (1964) The osmotic adjustment in the echinoderm, *Strongylocentrotus droebrachiensis*. *Comp Biochem Physiol* 13(3):205–216.

Supporting Information

Stumpp et al. 10.1073/pnas.1209174109

SI Validation of Selective Ion Electrode Measurements via BCECF in the Extracellular Matrix

To validate the selective ion electrode measurements, which were used to determine pH within the extracellular matrix (ECM), we additionally performed fluorimetric, noninvasive pH measurements using the pH-sensitive dye 2′,7′-bis-(carboxyethyl)-5(6)-carboxyfluorescein-acetoxymethylester (BCECF-AM) (Fig. S1).

Fluorimetric experiments were conducted as follows: To measure pH within the primary body cavity in larvae, we made use of xenobiotic transport—a mechanism usually used as a cellular defense mechanisms against toxins in aquatic organisms (multixenobiotic transport). Cleaved BCECF was exported from the cytosol of cells lining the gastric tract and subsequently trapped in the ECM of the body cavity. BCECF-AM (Invitrogen) stock solution of 10 mM in dimethyl sulfoxide (DMSO) (Invitrogen) was, in a first step, diluted with filtered seawater to 100 μM (1:100). Larvae (8–24 d postfertilization) were loaded with BCECF-AM in a second dilution step by mixing larval culture seawater including five to six individuals with BCECF/seawater solution. The final working solution had a BCECF concentration of 30 μM and a DMSO concentration of 0.3% (vol/vol). Animals were incubated in 30 μM BCECF-AM for 2 h at 12 °C in the dark. After incubation, larvae were washed five times with seawater and were kept at 12 °C in the dark for 60 min until fluorescence intensity in the primary body cavity was sufficient for detection. The procedure did not harm the animals: remaining individuals that were not used for the pH measurements survived a minimum of 7 d following the treatment. Late larvae (24 d postfertilization) close to settlement went through metamorphosis in the incubation tubes after the treatment with BCECF-AM.

pH_e measurements were conducted using an inverted confocal laser-scanning microscope (Leica; SP5) equipped with a perfusion system (comparable with the one used for the microelectrode measurements). Larvae were mounted in the perfusion bath at control $p\mathrm{CO_2}$ conditions (pH 8.1) and held in place with a glass holding pipette to which a slight vacuum was applied (Fig. S4). The bath (volume of 0.5 mL) was perfused at a rate of 3 mL $\mathrm{min^{-1}}$ with seawater adjusted to different pHs by injection of pure CO_2 (pH 8.1, 7.7, 7.3, and 6.9; temperature of 13 ± 0.2 °C). Each larva (n = 7) was left to adjust to pH 8.1 for 10 min before the first pH change was introduced. pH was changed in the order of 8.1, 7.7, 7.3, 6.9, and back to control pH 8.1. Each pH was applied for 10 min. One experiment lasted 60–65 min. The recording interval was once per minute for 5 min postsolution change, one recording at 7 min postsolution change, and one at 10 min postsolution change to minimize dye bleaching throughout the experiment. With selected confocal laser settings, no detectible dye bleaching occurred. Two larvae exposed to the same experimental protocol, but only supplied with seawater adjusted to pH 8.1, served as control for fluorescence intensity drift over the experimental period. This way, an increase or decrease in pH_e due to potential active regulation of the larvae in response to elevated $p\mathrm{CO_2}$ could be reliably detected. Because of high variations in fluorescence intensity ratios (ratios between 2.5 and 3.5) among individual larvae, data were normalized to the starting fluorescence intensity ratio at pH 8.1 of the respective larva.

For calibration of BCECF fluorescence intensity ratios, it was assumed that the extracellular fluid in the primary body cavity is similar in composition to seawater. BCECF-dextran (10 mM in dimethyl sulfoxide; Invitrogen) was diluted in artificial seawater adjusted to different pH to a final concentration of 50 μM. This concentration of BCECF-dextran yielded the same fluorescence intensity range when using the same confocal settings as BCECF-loaded larvae. To maintain stable pH values in seawater, artificial seawater (400 mM NaCl, 9.6 mM KCl, 52.3 mM $MgCl_2$, 9.9 mM $CaCl_2$, 27.7 mM Na_2SO_4) was buffered with 20 mM Tris·HCl. Measurements were conducted at 12 °C. For better comparison with values obtained in larvae, normalization was conducted by dividing all ratio values by the ratio measured at pH 8.1. The normalized ratio increased linearly with increasing pH up to a pH of 7.7. Between pH 7.7 and 8.1, almost no increase in ratio could be observed. This indicated a limited BCECF sensitivity for pH measurements in seawater.

The results confirm the high proton permeability of the ECM. However, as shown in the main article, the optimum range (linear part of the sigmoidal curve) for BCECF pH measurements in seawater lies between 6.5 and 7.5. Thus, the ratio changes for the pH steps 8.1–7.7 and 6.9 back to 8.1 have signal-to-noise ratios that prevent accurate measurements (Fig. S1).

For intracellular pH measurements using BCECF-AM, we removed the epithelial cells according to the description provided in the main article to reduce background noise. Clearly visible primary mesenchyme cells that were sufficiently loaded with the dye were used for the recordings (Fig. S5).

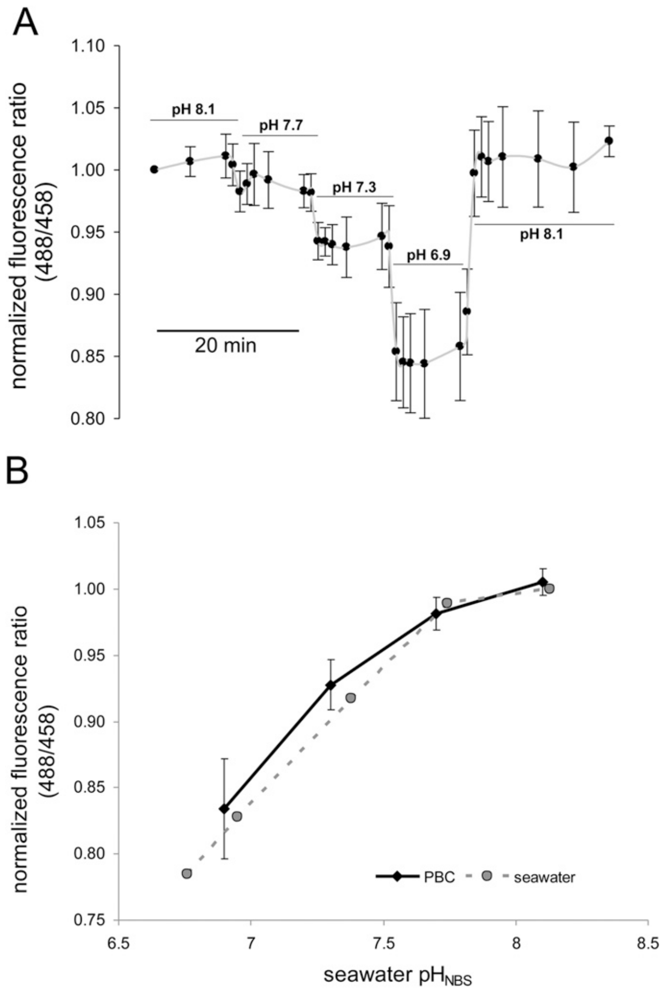

Fig. S1. Extracellular pH (pH$_e$) measurements in larvae of *Strongylocentrotus droebachiensis*. (*A*) BCECF fluorescence ratio is given as a measure of pH$_e$ at different seawater (bath) pH values relative to starting ratio. pH$_e$ follows seawater pH without significant compensation in the observation period. The effects are reversible without regulatory overshoot. (*B*) Correlation of fluorescence ratio from BCECF-dextran in seawater pH and BCECF-AM in PBC (n = 2 for BCECF-dextran in seawater; n = 7 for PBC measurements; mean ± SD). BCECF-dextran was normalized onto the ratio at pH 8.1. Note the decreasing slope of the calibration curve between pH 7.7 and pH 8.1 indicating the border of BCECF detection range in seawater similar to the slope decrease of the calibration curve of BCECF-AM in the primary mesenchyme cells (see *Results and Discussion* for details).

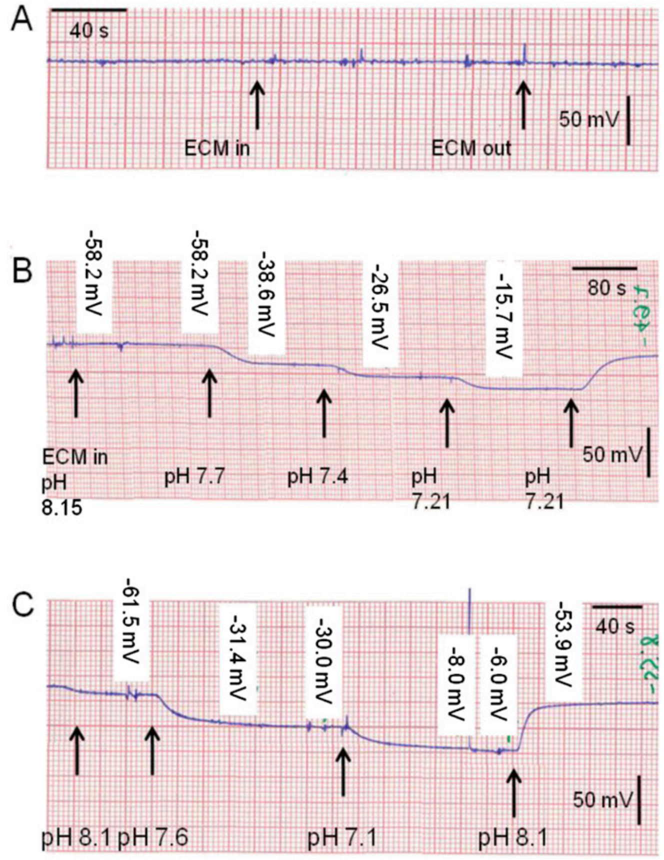

Fig. S2. Original recordings of voltage measurements (time line from *Left* to *Right*) using nonselective (*A*) or H^+-selective (*B* and *C*) microelectrodes. No potential difference was recorded during insertion of the electrode into as well as during removal from the ECM (*A*). pH steps recorded within the ECM demonstrating pH conformity to the environmental pH (*B*). pH steps recorded within the perfusion bath for electrode calibration (*C*). Note the slower response times within the ECM.

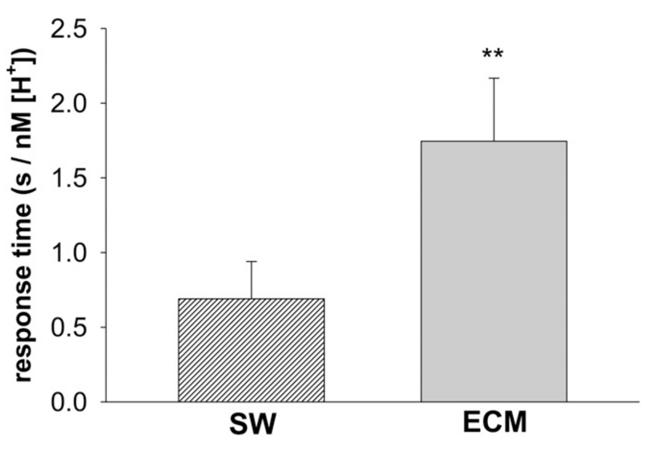

Fig. S3. Equilibration time of fluid exchange in the perfusion bath combined with the response time of the ion-selective electrode in seawater (SW) and within the extracellular matrix (ECM). Response time was calculated from the time needed to reach 95–100% of the fully stabilized value after a pH change between 8.1 and 7.2. For a linear relationship, differences in pH are expressed as H^+ concentrations. Bars represent ± SD; n = 10–12.

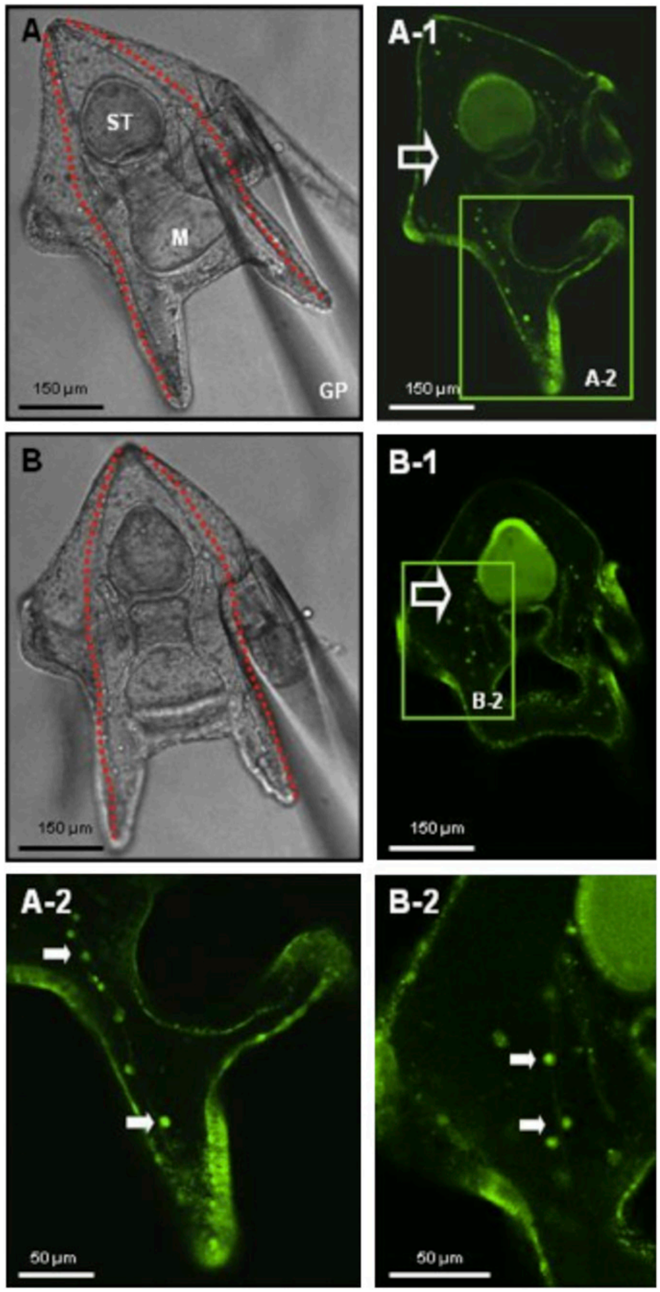

Fig. S4. In vivo confocal imaging of *S. droebachiensis* pluteus larvae (*A* and *B*). Primary mesenchyme cells along the calcitic spicules (PMCs, small arrows), the outer ectodermal epithelium, and digestive tract could be visualized in larvae loaded with BCECF-AM and exposed to probenecid. pH measurements in the extracellular environment directly surrounding the PMCs (large arrow) were performed with microelectrodes and microfluorimetrically (*SI Text*). The primary body cavity (large arrows) is filled with a collagen-glycoprotein matrix. GP, holding glass pipette; M, mouth; ST, stomach; spicules are traced in red.

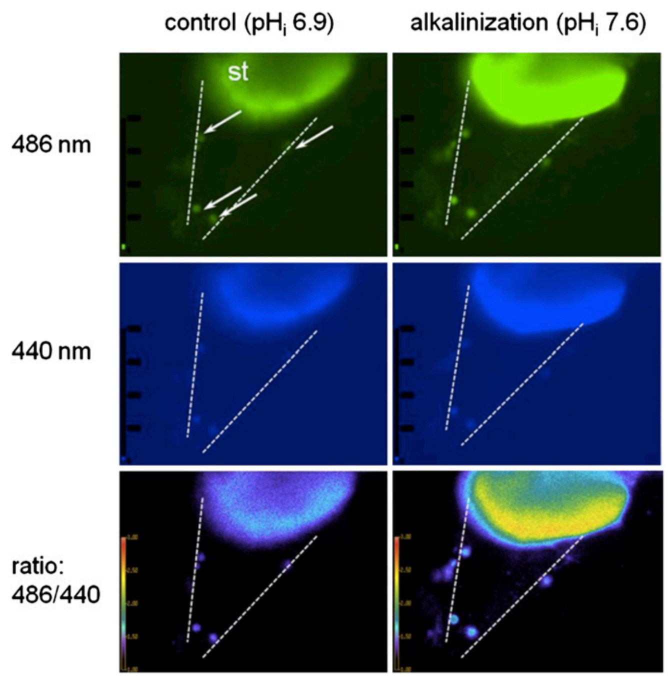

Fig. S5. Selected pseudo color images during BCECF recordings at 486-nm (first row) and 440-nm (second row) excitation and of the emission ratio (third row). A strong signal was emitted by the stomach (st) cells, which were clearly separated from the primary mesenchyme cells (indicated by arrows). During NH_3/NH_4^+-induced alkalosis, ratios increased steadily, corresponding to a rise in pH from pH$_i$ 6.9 until the plateau was reached at pH$_i$ 7.6. The dashed lines indicate the location of the two spicules.

Table S1. Intracellular pH values from microfluorimetry experiments

Baseline pH$_i$	Treatment after prepulse	Acidosis pH$_i$	Recovery pH$_i$	Recovery ΔpH$_i$	Recovery rate, ΔpH$_i$ min^{-1}	*n*
7.18 ± 0.20	ASW	6.50 ± 0.06	7.13 ± 0.20	0.64 ± 0.17	0.047 ± 0.011	5
6.82 ± 0.16*	5 mM Na^+	6.32 ± 0.10**	6.44 ± 0.06**	0.13 ± 0.05**	0.015 ± 0.009**	5
6.64 ± 0.22	ASW	6.34 ± 0.16	6.58 ± 0.17	0.25 ± 0.07	0.041 ± 0.009	4
6.71 ± 0.22	0 mM HCO_3^-	6.40 ± 0.15	6.42 ± 0.15	0.02 ± 0.01**	0.008 ± 0.007**	4
6.77 ± 0.19	ASW	6.40 ± 0.21	6.71 ± 0.19	0.32 ± 0.04	0.042 ± 0.023	4
6.96 ± 0.28	amiloride	6.55 ± 0.34	6.72 ± 0.31	0.17 ± 0.11*	0.033 ± 0.015	5

Comparison of pH$_i$ values, changes (ΔpH), and recovery rates (ΔpH$_i$ min^{-1}), after NH_4Cl withdrawal from experiments as shown in Fig. 5. *$P < 0.05$; **$P < 0.01$.

Table S2. Seawater physicochemical conditions

Incubation group	Temperature, °C	Salinity	pH	Ω_{Ca}	Ω_{Ar}	CO_2, ppm	C_T
Control	9.42 ± 0.95	31.7 ± 0.14	8.06 ± 0.02	3.84 ± 0.30	2.42 ± 0.19	449.7 ± 45.4	2,582.1 ± 13.4
CO_2, ~1,120 ppm	9.43 ± 0.96	31.7 ± 0.09	7.73 ± 0.03	1.94 ± 0.04	1.22 ± 0.02	1,015.1 ± 12.4	2,695.9 ± 42.4
CO_2, ~2,400 ppm	9.48 ± 0.94	31.8 ± 0.08	7.39 ± 0.02	0.88 ± 0.01	0.55 ± 0.01	2,457.8 ± 17.0	2,839.4 ± 23.7

Seawater physicochemical conditions during hypercapnia experiments (10 d each). C_T, total dissolved inorganic carbon; Ω_{Ca}, calcite saturation state; Ω_{Ar}, aragonite saturation state; pCO_2, partial pressure of CO_2;. Values are presented as mean ± SD.

Table S3. Artificial seawater solutions

	ASW	20 mM NH_3/NH_4^+	5 mM Na^+	0 BIC	ASW_{Nig}
Na^+	420	430	5	474	370
K^+	9.9	9.9	9.9	9.9	150
Mg^{2+}	53.3	48.3	53.3	53.3	53.3
Ca^{2+}	15.3	9.9	10.3	9.9	10
Cl^-	468.6	490	488.6	519.3	555.3
SO_4^{2-}	28.2	28.2	28	28	28
HCO_3^-	2.35	2.35	2.35	0	0
NH_4^+		20			
$NMDG^+$			443		
Hepes				5	
pH	8.2	8.2	8.2	8.2	
Osmolality	970 ± 10	971 ± 10	972 ± 10	973 ± 10	974 ± 10

Artificial seawater (ASW) solutions (concentrations given in $mmol \cdot kg^{-1}$).